

## Recent progress on nucleon form factors

---

**Dalibor Djukanovic**<sup>a,\*</sup>

<sup>a</sup>*Helmholtz Institute Mainz, Staudingerweg 18, D-55128 Mainz, Germany  
GSI Helmholtzzentrum für Schwerionenforschung, D-64291 Darmstadt, Germany*

*E-mail:* [d.djukanovic@him.uni-mainz.de](mailto:d.djukanovic@him.uni-mainz.de)

The form factors of the nucleon provide key information on nucleon properties. When confronted with precisely measured observables from experiments, they serve as benchmark quantities for lattice calculations. On the other hand lattice determinations may serve as vital theory input for the interpretation of experiments, e.g. in neutrino-nucleus scattering. I review recent progress in the calculation of nucleon form factors on the lattice and its relevance to future experiments.

*The 38th International Symposium on Lattice Field Theory, LATTICE2021 26th-30th July, 2021  
Zoom/Gather@Massachusetts Institute of Technology*

---

\*Speaker

## 1. Introduction

Form factors encode fundamental properties of the nucleon, parametrizing its response to external currents, which are uniquely defined through their quantum numbers. We can derive basic properties of the nucleon from these form factors, e.g. charges, charge distributions, stiffness or rigidity. Thus a first principle calculation from lattice Quantum Chromodynamics (QCD) gives us a key insight into the strong interactions governing the forces inside nucleons. A detailed knowledge of the nucleon form factor is vital to the success of upcoming high precision experiments involving nuclear targets like DUNE at Fermilab [1] or Hyper-Kamiokande [2]. Recent progress in nucleon form factor calculations suggests a number of areas, where the lattice may have an immediate impact, e.g.

- in searches for beyond Standard Model (BSM) physics,
- as high precision input in analysis of experimental data,
- in cases where there is disagreement between different experiments.

The first point is mostly the domain of the nucleon form factors at vanishing momentum transfer (charges). Restricting models of BSM physics one needs the corresponding matrix elements of non-Standard Model hadronic currents in order to establish strong bounds from experiments (c.f. [3]). Moreover, the axial charge is very well determined experimentally and serves as a benchmark quantity for extraction techniques on the lattice, where remarkable precision has been reached [4]. In dark matter searches the matrix element of the scalar current, the sigma term, plays an important role. There is a particularly interesting connection between the sigma term and  $\pi N$  scattering, via the Cheng-Dashen theorem [5], that enables direct comparisons of this quantity to dispersive (experimental data driven) determinations [6]. The sigma term is especially intriguing, since there is a slight tension between the dispersive analysis of [6] and the  $N_F = 2 + 1$  average of lattice determinations [7]. A very recent analysis [8] suggests that the tension might be due to excited-state contributions highlighting not only the need for statistical precision but for a high level of control over systematics.

Also the case of non-vanishing momentum transfer is highly interesting, not only for nucleon properties, but also in BSM physics searches and high precision determinations of SM observables at low energies. In the upcoming experiments at DUNE [1] the axial form factor of the nucleon plays a crucial role for the interpretation of the data, especially in the region, where quasi-elastic neutrino-nucleus scattering is the dominant process (c.f. [9]). A determination of the axial radius to 20% accuracy is sufficient to render the theoretical uncertainty due to  $r_A$  in neutron quasi-elastic cross sections to a subdominant contribution [10]. Here not only the radius is of interest but rather the whole  $Q^2$  dependence of the form factor.

The increase in precision opens up new windows of opportunity to determine SM parameters, such as the Weinberg angle, in low energy experiments, e.g. by measuring the weak charge of the proton in parity-violation experiments like P2 at MESA [11] or Q-weak at JLAB. Here a detailed knowledge of the strange electromagnetic form factors is an important ingredient in the extraction of the weak charge [12].

One of the opportunities where lattice determinations may hope to resolve a persisting discrepancy is the proton radius. For the proton radius experimental data from  $ep$ -scattering [13] and spectroscopy measurements of muonic hydrogen Refs. [14, 15] are at odds. A recent measurement of the proton radius, again from  $ep$ -scattering, seems to favor the smaller radius [16], which is also consistent with dispersive analysis (c.f [17]).

The impact of the lattice crucially depends on the achievable accuracy, not only in terms of statistical precision, but to which degree all relevant systematics are understood and under control. There has been quite some progress in the last few years concerning both and I review the current status of affairs, focusing on the vector- and axialvector form factors.

In an effort to make this proceeding self-contained I first give an overview of the methods used in the extraction of the nucleon form factors. For a very recent more detailed account I refer to last years' conference proceeding [18]. In the third section I highlight possible sources of systematic uncertainty. Finally I summarize the most recent result for the vector and axialvector form factors.

## 2. Lattice methodology

The quantities calculated on the lattice are euclidean  $n$ -point correlation functions of hadronic operators, where the nucleon is created (annihilated) via an interpolating source (sink) operator  $\bar{\Psi}(\Psi)$  typically of the form

$$\Psi_\alpha(x) = \epsilon_{abc} \left( u_a^T(x) C \gamma_5 d_b(x) \right) u_{c,\alpha}(x), \quad (1)$$

where  $C$  is the charge conjugation matrix,  $u$  and  $d$  denote the up and down quarks.

In the time-momentum representation the spin-projected two-point function is then given by

$$C_2(t; \mathbf{p}) = \Gamma_{\alpha\beta} \sum_{\mathbf{x}} e^{-i\mathbf{p}\mathbf{x}} \left\langle \Psi_\beta(\mathbf{x}, t) \bar{\Psi}_\alpha(0) \right\rangle, \quad (2)$$

where the source is shifted to the origin. Inserting a complete set of energy-eigenstates the spectral decomposition of the two-point function reads

$$C_2(t; \mathbf{p}) = \sum_n \underbrace{|\langle n | \Psi | N \rangle|}_{Z_n} e^{-E_n t}, \quad (3)$$

where all states  $|n\rangle$  compatible with the quantum numbers of the interpolating operator, i.e. beyond the ground state also excited and multi-particle states, contribute. The exponential falloff leads to a suppression of excited states for large enough distances between source and sink. In this region the dominant contribution to the correlation functions comes from the ground state and its properties are readily read off, e.g. as plateaus in effective mass plots defined via

$$E_{\text{eff}} = \frac{1}{\tau} \ln \frac{C_2(t; \mathbf{p})}{C_2(t + \tau; \mathbf{p})}. \quad (4)$$

Unfortunately baryons are affected by an infamously unfavorable signal to noise ratio, which effectively drowns the signal in noise once the ground state would start to dominate. One may intuitively understand this looking at the variance directly calculated using the interpolating operator

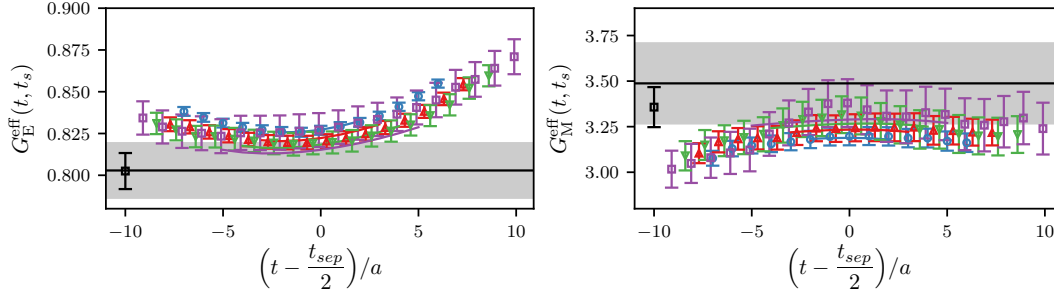


**Figure 1:** Effective form factor for the electric (left) and magnetic (right) isovector vector current, on ensemble D200 at first non-vanishing momentum transfer (figure taken from Ref. [28]). The effective form factor is plotted for different values of  $t_{\text{sep}}$  between 1 and 1.5 fm, together with the estimate of ground state matrix element from the direct fits including excited states (black data points) and the summation method result (gray band).

of Eq. (1) (c.f. Ref. [19]). One possible contraction of the squared operator results in three pions propagating from source to sink, thus the variance in the large time separation limit reads

$$\frac{\Delta C_2(t; \mathbf{0})}{C_2(t; \mathbf{0})} \sim \frac{\exp(-\frac{3}{2}m_\pi t)}{\exp(-m_n t)}. \quad (5)$$

Therefore in the asymptotic limit the noise grows exponentially. In order to reach the ground state region earlier, effectively taming the signal-to-noise problem, smearing techniques are used which lead to an increased overlap of the interpolating operator with the ground state [20–22]. The signal-to-noise problem is exacerbated in the case of the three-point functions, where the computationally feasible source-sink separations are severely limited by the dramatic increase in cost. Moreover in the contractions pertinent to form factor calculations, so-called quark-disconnected contributions may arise, which are notoriously difficult to calculate. Most simulations use degenerate light quarks, which in some of the isovector combinations happen to be free of quark-disconnected contributions. However this is not true for all, e.g. the strange electromagnetic form factor, and for the flavor decomposition the isoscalar form factors are still needed, which receive contributions from these types of diagrams. For the calculation of the connected diagrams most analyses use the sequential inversion method with a fixed sink, i.e. located at a fixed time separation to the source. While in this setup for every source-sink separation and every sink momentum an explicit inversion is needed, the correlator for all operator insertions between source and sink are accessible without further inversion. The statistical precision is usually increased using variance reduction techniques such as all mode averaging [23, 24]. In recent years algorithmic developments, e.g. hierarchical probing [25], low mode deflation [26], frequency-splitting [27] to name a few, have cut the cost for the calculation of disconnected diagrams dramatically.

For the form factor calculations the extractions usually proceed via the ratio of two- and three-point functions, where the ratio is constructed such that overlap factors cancel and the ground state matrix element is dominant.

In most studies one of the following ratios is used [29, 30]

$$R^X(t, t_s; \mathbf{q}) = \frac{C_3^X(t, t_s; \mathbf{q})}{C_2(t_s; \mathbf{0})} \sqrt{\frac{C_2(t_s - t; -\mathbf{q}) C_2(t, \mathbf{0}) C_2(t_s; \mathbf{0})}{C_2(t_s - t; \mathbf{0}) C_2(t; -\mathbf{q}) C_2(t_s; -\mathbf{q})}}, \quad (6)$$

$$R^X(t, t_s; \mathbf{q}) = \frac{C_3^X(t, t_s; \mathbf{q})}{C_2(t_s; \mathbf{0})}, \quad (7)$$

where the nucleon three-point-function of a general operator  $X$  is given by

$$C_3^X(t, t_s; \mathbf{q}) = \Gamma_{\alpha\beta} \sum_{\mathbf{x}, \mathbf{y}} e^{i\mathbf{q}\mathbf{y}} \langle \Psi_\beta(\mathbf{x}, t_s) X(\mathbf{y}, t) \bar{\Psi}_\alpha(0) \rangle. \quad (8)$$

For vanishing momentum transfer the ratios coincide, however for non-vanishing momenta the overlap factors of the two-point functions do not cancel for the latter. Matching the spectral representation of the ratios in Eqs. (6,7) to the corresponding nucleon matrix elements parameterized using form factors, one obtains effective form factors (see Fig. 1).

In the fixed sink method the nucleon at the sink is usually at rest, i.e. for a momentum transfer  $\mathbf{q}$  the initial and final nucleon states have momenta

$$\mathbf{p}' = 0, \quad \mathbf{p} = -\mathbf{q}. \quad (9)$$

The operator  $X$  is the current operator, which is classified with respect to its symmetry as

$$X_\mu^V(x) = \bar{q}(x) \gamma_\mu q(x), \quad (10)$$

$$X_\mu^A(x) = \bar{q}(x) \gamma_\mu \gamma_5 q(x), \quad (11)$$

$$X^S(x) = \bar{q}(x) q(x), \quad (12)$$

$$X_{\mu\nu}^T(x) = \bar{q}(x) \sigma_{\mu\nu} q(x), \quad (13)$$

for the vector, axial, scalar and tensor currents, respectively. Also non-local operators are used, e.g. point-split currents in the vector case resulting in conserved charges.

### 3. Sources of systematics

The most severe problem every lattice calculation of the nucleon form factors faces is that of excited states. While in the asymptotic limit of large euclidean time separations ratios like Eq.(6) are proportional to the ground state hadronic matrix element we are after, the computationally affordable  $t_{\text{sep}}$  are such that there still is sizable contamination left from excited states (see Fig. 1). One obvious remedy is to simply keep more terms in the spectral decomposition of the two- and three-point functions

$$C_2(t; \mathbf{p}) = |Z_0(\mathbf{p})|^2 \exp[-E_0(\mathbf{p})t] + |Z_1(\mathbf{p})|^2 \exp[-E_1(\mathbf{p})t] + \dots, \quad (14)$$

$$\begin{aligned} C_3(t, t_{\text{sep}}; \mathbf{p}', \mathbf{p}) &= Z_0(\mathbf{p}') Z_0^*(\mathbf{p}) \langle 0|X|0 \rangle \exp[-E_0(\mathbf{p}')(t_{\text{sep}} - t)] \exp[-E_0(\mathbf{p})t] \\ &+ Z_0(\mathbf{p}') Z_1^*(\mathbf{p}) \langle 0|X|1 \rangle \exp[-E_0(\mathbf{p}')(t_{\text{sep}} - t)] \exp[-E_1(\mathbf{p})t] \\ &+ Z_1(\mathbf{p}') Z_0^*(\mathbf{p}) \langle 1|X|0 \rangle \exp[-E_1(\mathbf{p}')(t_{\text{sep}} - t)] \exp[-E_0(\mathbf{p})t] \\ &+ Z_1(\mathbf{p}') Z_1^*(\mathbf{p}) \langle 1|X|1 \rangle \exp[-E_1(\mathbf{p}')(t_{\text{sep}} - t)] \exp[-E_1(\mathbf{p})t] + \dots, \end{aligned} \quad (15)$$

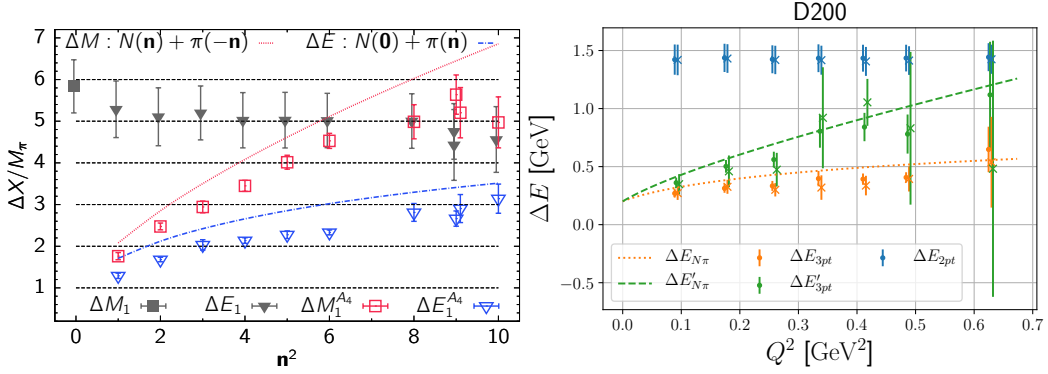


**Figure 2:** Plots showing the different values of the energy gap to the first excited state, when fitted to the two- or three-point functions. The figures originally were published in [32] (left) and [33] (right), and are reproduced under the Creative Commons Attribution 4.0 International license.

to fit all available data. In principle the overlaps  $Z_i$  and the energies  $E_i$  are universal and one may try to fix these in fits to the two-point functions first, in turn to be used as *fixed parameters* for higher  $n$ -point functions [31]. Obtaining the excited-state parameters from fits to the two-point functions is a daunting task given the signal-to-noise problem. There is evidence that, at least for some observables, this procedure might not be best suited to account for the excited-state effects found in the three-point functions. The excited state properties as extracted from the two- and three-point functions can differ significantly, as has been observed especially in the axialvector sector [32–34] (see Fig. 2). One alternative is to perform simultaneous fits of two- and three-point functions fitting the excited state properties as nuisance parameters. Given the large number of data points that enter in such fits estimating the covariance matrix is very challenging and the resulting procedure may become unstable. Also the current level of statistics might not be sufficient to consistently extract all the excited-state parameters from two- and three-point functions. Alternatively an intermediate approach between fixing the excited state parameters completely from the two-point functions and simultaneous fits leaving them open is to use prior knowledge about the energies and overlaps, with some freedom for the higher  $n$ -point function to still choose a different value. While the gaps and overlaps may be universal it is by no means clear that the correlation functions exhibit that pattern. We could find ourselves in a situation where a multitude of excited states might be subsumed into one *effective* excited state that bares no resemblance to the one from the two-point functions. The prior information might come from a simple ansatz about the excitation spectrum of the interpolating operators, e.g. non-interacting multi-particle states of nucleons and pions or refinements including interactions [35]. One may also resort to estimates based on chiral perturbation theory about the size of the excited state contaminations [36, 37] which predicts the dominant contribution to come from pion-nucleon states<sup>1</sup>. In fact the energy of the first excited state as extracted from the two-point functions reported in recent studies is much higher than expected from a chiral analysis and is closer to the Roper mass  $N(1440)$ , e.g. [34], or even heavier resonances like  $N(1710)$  [32]. Most recently the excited state analysis has been extended to non-vanishing momentum transfer for the axialvector

<sup>1</sup>In ratios like Eq. (6) no new parameter enter the ChPT prediction of excited states if the smearing size of the interpolating operator is small compared to the inverse pion mass [37].

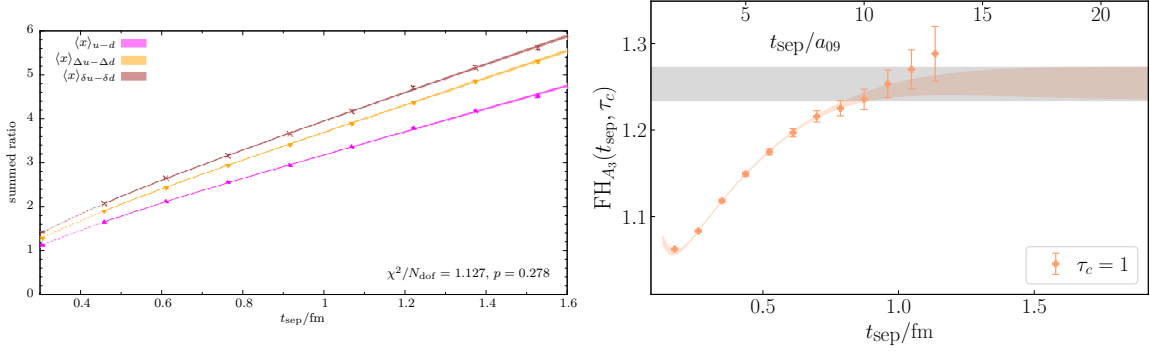


**Figure 3:** Examples for the extension of the summation method to smaller values of  $t_{\text{sep}}$  for the twist-2 operators (left) and the Feynman-Hellmann correlator of the third component of the axial current [46]. The figures originally were published in this conference proceedings [47] (left) and in Ref. [46] (right), and are reproduced under the Creative Commons Attribution 4.0 International license.

[38] and vector currents [39], where the induced pseudoscalar form factor  $G_P$  is shown to receive strong corrections. While these analyses work best for larger source-sink separation than usually available, they still serve as a good indication about the expected size of these corrections.

Another approach dealing with excited states is given by the summation method [40], which has a long history in the calculation of nucleon form factors [41–45]. Here one sums the correlators for timeslices between source and sink, which leads to a parametric suppression of excited states with  $t_{\text{sep}}$  instead of  $t$ ,  $(t_{\text{sep}} - t)$ . To illustrate this let us write a correlation function that has been constructed such that the leading exponential falloff is cancelled and  $\Delta(\Delta')$  denote the energy gap of the excited to the ground state emanating from source (sink), i.e.

$$C(t, t_{\text{sep}}; \mathbf{p}) = C_0 + C_1 \exp[-\Delta t] + c \exp[-\Delta'(t_{\text{sep}} - t)] \quad (16)$$

$$S(t_{\text{sep}}) = \sum_{t=t_{\text{skip}}}^{t_{\text{sep}}-t_{\text{skip}}} C(t, t_{\text{sep}}; \mathbf{p}) = C_0 \frac{t_{\text{sep}} - 2t_{\text{skip}} + a}{a} + C_1 \frac{\exp[-\Delta t_{\text{skip}}] - \exp[-\Delta(t_{\text{sep}} - t_{\text{skip}} + a)]}{1 - \exp[-\Delta a]} + \dots, \quad (17)$$

where in the last line we see that the exponential falloff is enhanced compared to Eq. (16). One welcome simplification of this method is the reduction in data size, leading to more stable estimates of covariance matrices. Moreover, taking the derivative of Eq. (17) with respect to  $t_{\text{sep}}$  the region of ground state dominance is marked by a plateau and one has the opportunity to *monitor* the window for which a stable extraction is possible even for lower values of  $t_{\text{sep}}$  [46] (see Fig. 3). In any case the identification of the ground state matrix element is a challenging task. For some observables one may resort to constraints based on symmetries, that various extractions of ground state matrix elements have to fulfill once the asymptotic regime has been reached. One such constraint is given by the PCAC relation, which has to be fulfilled on the correlator level. Any deviation in such relations for the extracted ground state matrix elements may be indicative for a failure to cleanly separate the excited-state contributions (c.f. [32, 33, 48]). For observables where symmetry constraints are not easily established the best option is to look for a consistent value through various methods.

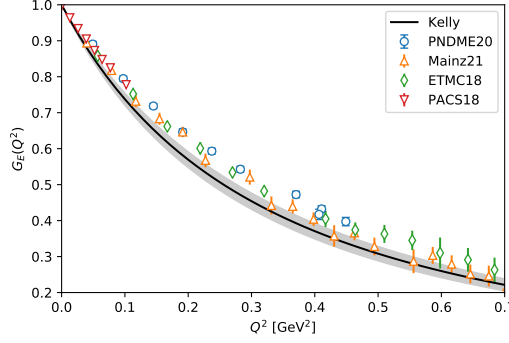


**Figure 4:** Compilation of the isovector electric Sachs form factor for physical pion mass ensembles, where Kelly denotes the parametrization from [52], and the lattice data are taken from Ref. [31] blue circles (PNDME20), Ref. [28] orange upwards triangles (Mainz21), Ref. [53] green diamonds (ETMC18) and Ref. [54] red downward triangles (PACS18).

Besides the excited-state contributions one major source of uncertainty is due to discretization and the finite size of the simulated boxes. A controlled extrapolation to the continuum and infinite volume has to be performed. Another immediate consequence of the discretization is that momenta are not continuous. When we are interested in the  $Q^2$  dependence of the form factors, or quantities defined via the slope (at vanishing momentum), an interpolation of the simulated points is needed. This is also true in the continuum when one has to fit the available experimental data. It is natural to use the same approaches as in experiments, and indeed most analysis adopted multiple strategies ranging from historically motivated fit forms like dipole, or Padé fits, model-independent approaches like  $z$ -expansion [49] or effective field theory approaches using chiral perturbation theory results (e.g. [50]). Some observables may depend strongly on the actual fit form used, e.g. the dipole fits, being the least flexible, usually tend to give the smallest error. However in [51] the dipole was found to potentially suffer from a large bias if the true model is in fact not of dipole form. Most recent lattice studies quote results for the  $z$ -expansion. To be more specific the dipole or  $z$ -expansion [49] is given by

$$G_{A/E/M}^{\text{dipole}}(Q^2) = \frac{a_{A/E/M}}{\left(1 + \frac{Q^2}{M^2}\right)^2}, \quad (18)$$

$$G_{A/E/M}(Q^2) = \sum_{k=0}^{\infty} a_k z(Q^2)^k, \quad (19)$$

with

$$z(Q^2) = \frac{\sqrt{t_{\text{cut}} + Q^2} - \sqrt{t_{\text{cut}} - t_0}}{\sqrt{t_{\text{cut}} + Q^2} + \sqrt{t_{\text{cut}} - t_0}}, \quad (20)$$

where  $t_{\text{cut}}$  is the branch cut for the respective form factor and  $t_0$  is a free parameter corresponding to the point in  $t$  that maps onto  $z = 0$ . The dipole is motivated mostly by its simplicity and phenomenological success, whereas the  $z$ -expansion is based on a conformal mapping, constructed

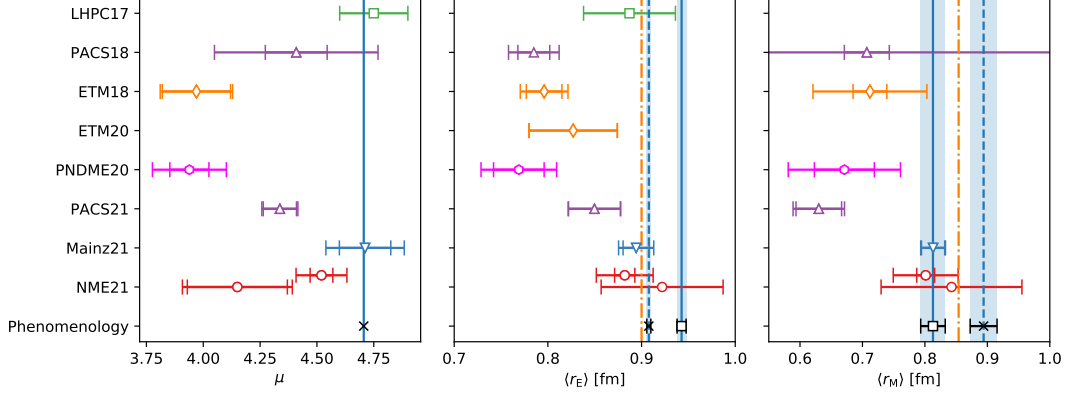


**Figure 5:** Comparison of recent lattice determinations, from Ref. [48] red circle (NME21), Ref. [31] magenta hexagon (PNDME20), Refs. [53, 55] orange diamond (ETM18/20), Ref. [28] blue downwards triangle (Mainz21), Refs. [54, 56] purple upwards triangle (PACS18/21), Ref. [57] green squares (LHPC17), for the isovector magnetic moment, electric and magnetic radius, respectively. The yellow dash-dotted lines correspond to the dispersive analysis of Ref. [17]. The phenomenological values for the magnetic moment is derived from the proton and neutron values taken from PDG [58]. The black square denotes the electromagnetic radii corresponding to a value derived from Mainz/A1 [13] data for the proton. Alternatively the crosses denote the derived values using, for  $\langle r_E \rangle$  the CODATA2018 value of the proton electric radius, and for the  $\langle r_M \rangle$  the world data excluding Mainz/A1. In both cases the values for the neutron are taken from [58].

such that one obtains the largest possible range of convergence for the form factors, treated as a function of complex arguments. Here the cut on the real axis, i.e. the threshold of (multi-)particle production, is accounted for and amounts to  $\sqrt{t_{\text{cut}}} = 3m_\pi(2m_\pi)$  in the axialvector (vector) current case. For any parametrization interpolating between simulated points there is usually two ways the analysis may proceed. In one approach the dipole or  $z$ -expansion fits are used to estimate derived quantities, like radii, for fixed simulation parameters and subsequently chiral and continuum fits are performed on these. Alternatively the  $z$ -expansion formula may be amended with terms parametrizing the chiral and discretization effects [31]. In this immediate form the number of data points that constrain the fit parameters is larger compared to the two step process, and one may hope for more stable fits, especially for the cases where one includes lattice spacing and finite volume effects simultaneously. For  $z$ -expansion fits most studies obtain stable results only to a low order in  $z$  ( $k \leq 2$ ), stabilizing the fits with gaussian priors for the higher order coefficients. The magnetic form factor is especially difficult as lattice studies do not have a handle on the point at  $Q^2 = 0$ , leading to somewhat larger uncertainties in the estimates of the magnetic moment and radius. Another idea was pursued in Ref. [28], where formulae based on an effective field theory description are used [50] to perform  $Q^2$ -, chiral- and continuum extrapolations in one global analysis. In general the range of pion masses for which the chiral extrapolations converge is not known, and cuts with respect to the pion mass should be performed to assess potential bias. Most recently there is also direct determination of the radius implementing the derivative on the correlator level [55, 56] eliminating the modeling of the  $Q^2$  dependence as a source of systematic uncertainty.

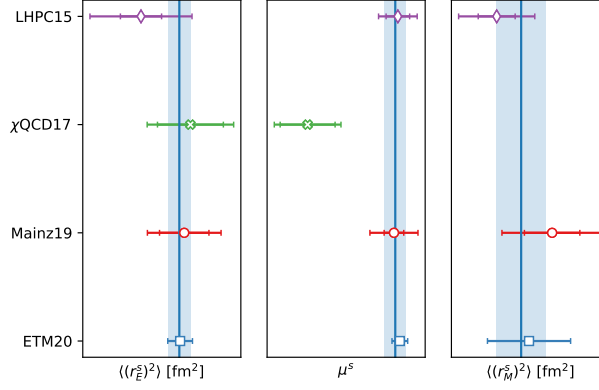


**Figure 6:** Comparison of the strange electromagnetic form factor of the nucleon, data are from Ref. [61] purple diamonds (LHCPC15), Refs. [62, 63] green crosses ( $\chi$ QCD17), Ref. [64] red circle (Mainz19), and Ref. [65] blue squares (ETM20). The blue shaded area is the PDG-style unconstrained weighted average.

The possible variations in the analysis can become quite numerous and it is not clear from the start which variations really have a strong effect in the final observable. Therefore choices have to be made in the course of the analysis to keep the number of variations manageable. Once the number of different methods is fixed one still faces the problem of obtaining a final estimate from a range of determinations. Most studies proceed to give a best estimate of one favored model with a statistical error and an error based on variations of the analysis most sensitive to one of the aforementioned sources of systematic uncertainty. While for the statistical error resampling techniques are the de facto standard, for the latter no unified approach exists and various methods are applied in the literature. Some studies use the spread in the mean values of the variations to assign a systematic error, e.g. the error is large enough to cover all mean values of the variations. Another possibility is not to select a preferred model but to perform model averages using information criteria like the Akaike Information Criterion [59]<sup>2</sup>. Even cuts performed on the data, e.g. in  $Q^2$ ,  $m_\pi L$  or  $m_\pi$ , may be reinterpreted as a model selection problem [60] and can be included in such an average.

#### 4. Recent results

In Fig. 4 I show a compilation of the isovector electric Sachs form factor for close to physical pion mass ensembles. For most of the  $Q^2$  values the different extractions agree reasonably well within errors, where the data from PNDME [31] lies somewhat higher. The different analysis treat excited states differently, e.g. for Ref. [28] data from the two-state fits with narrow priors, obtained from two-state fits, are shown. The effective form factors in Ref. [54] have been extracted using plateau fits. In Ref. [53] the ground state matrix element was identified by two-state fits, however demanding consistency between determinations based on two-state fits and the plateau method for several  $t_{sep}$ . For Ref. [31] the excited state energy gaps from the two-point functions were used as fixed input in the three-point function (data for a09m130W is shown). In Fig. 5 I show a

<sup>2</sup>In the case one model is clearly preferred by the AIC the model average effectively becomes a model selection.

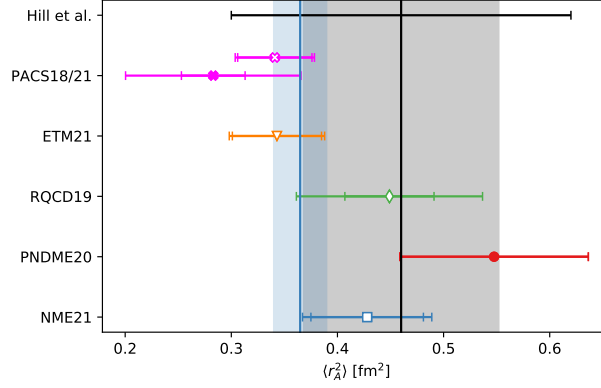


**Figure 7:** Comparison of lattice determinations of the axial radius  $\langle r_A^2 \rangle$ , from Ref. [48] blue square (NME21), Ref. [32] red circle (PNDME20), Ref. [33] green diamond (RQCD19), Ref. [34] orange triangle (ETM21), Refs. [54, 56] magenta cross (PACS18/21). The point labeled Hill et al. is an average of the values obtained from z-expansion fits to neutrino scattering and muon capture [10], with the grey band indicating a 20% error for  $\langle r_A^2 \rangle$ . The blue band is the unconstrained weighted average over the data points with open symbols, i.e. the most recent more precise data sets which quote a systematic error.

comparison of the latest results for the isovector magnetic moment and electromagnetic radii of the nucleon. The errors for the magnetic moment and radius are in general larger, mostly due to the missing point at vanishing momentum transfer and the associated extrapolation. It is also visible that reproducing the magnetic moment already is a challenge for lattice determinations. One may combine the experimentally available values for the proton radius from  $ep$ -scattering of Ref. [13] and from muonic hydrogen, with the experimentally known values for the neutron to obtain a data driven estimate of the isovector quantity, labelled *Phenomenology* in Fig. 5, for both cases. For the electric radius we see that most lattice determination are comparatively low. While there is a tendency towards the smaller value of the electric radius the  $ep$ -scattering value of Ref. [13] cannot be ruled out. A decisive statement about the proton radius puzzle is not yet possible. An interesting observation is that there seems to be a slight tension for the magnetic radius from the dispersive analysis [17] and the lattice determination of [28], while there is good agreement for the electric radius between the two.

For the case of the strange electromagnetic form factor I show a comparison in Fig. 6. While for the strange magnetic moment there is some tension between  $\chi$ QCD and the other estimates [61, 64, 65], the electric and magnetic radii agree very well amongst the different lattice determinations. The blue shaded area in Fig. 6 shows the PDG-style unconstrained weighted average, where I added the systematic errors in quadrature. This simple average reads

$$\mu^{s,\text{average}} = -0.0193(54), \quad (21)$$

$$\langle (r_E^s)^2 \rangle^{\text{average}} = -0.00484(54) \text{ fm}^2, \quad (22)$$

$$\langle (r_M^s)^2 \rangle^{\text{average}} = -0.0167(53) \text{ fm}^2. \quad (23)$$

A comparison of recent results for the axial radius is shown in Fig 7. All determinations individually meet the criterion of 20% error for  $r_A^2$ , with respect to the statistical error, put forth to

render the axial radius uncertainty a subleading effect in the cross section of quasi-elastic neutrino-nucleus scattering. The data depicted by open symbols agree within errors once the systematic error is added in quadrature. The blue shaded area is the unconstrained weighted average of these data points [33, 34, 48, 56], derived from  $z$ -expansion or direct extractions, with systematic errors added in quadrature, leading to a simple PDG-style average of

$$\langle r_A^2 \rangle^{\text{average}} = 0.365(25) \text{ fm}^2. \quad (24)$$

Let me stress that this average does not include any quality criteria with respect to the assessment of systematic errors. The systematics for the individual lattice determinations are very different, e.g. in Ref. [33] an extraction based on a dipole parametrization of the  $Q^2$  behavior gives a considerably smaller value, whereas in [56] the radius is obtained implementing the derivative directly.

## 5. Summary

Excited-state contaminations remain the most dominant source of systematic uncertainty for the form factors of the nucleon. Most analysis use multi-state fits to account for the effect of excited states at the correlator level, with a varying degree of prior knowledge applied to guide and stabilize procedures. Alternatively the summation method is used, where a comparable level of precision is usually achieved only with the extension of this method to include smaller source-sink separations below 1 fm. In the absence of a superior method for dealing with excited states, or more detailed knowledge of the excitation spectrum of the nucleon, it is important to show for every analysis that residual effects are under control. To that end one ideally performs several variations designed to elucidate the influence of the various systematics. Averaging the results of these variations based on AIC weights could provide an efficient way to establish the effects of systematics on the final observable.

In recent studies the effect of excited states was observed to be amplified in the case of the axialvector current. While the extractions for the axial radius seem to have reached the level of accuracy needed for example for the analysis of neutrino-nucleus scattering, further corroboration of the results is desirable to increase confidence that indeed all systematics are well under control.

The strange electromagnetic form factors of the nucleon, a key ingredient in the analysis of low energy parity-violation experiment, are in good agreement between the different lattice determinations, resulting in non-zero values for the strange magnetic moment and electromagnetic radii. More recently in Ref. [66] the strange axial form factor has been determined at physical pion mass. The systematic uncertainties in this quantity need to be further investigated.

Even though there is strong indication for a smaller value of the electric radius of the proton, as determined from muonic hydrogen, lattice determinations at the current level of statistics and systematics may not rule out the  $ep$ -scattering value of [13] with a high level of confidence. For an improved extraction, especially of the magnetic radius, more data points at low  $Q^2$  are needed.

## References

- [1] DUNE collaboration, *Long-Baseline Neutrino Facility (LBNF) and Deep Underground Neutrino Experiment (DUNE): Conceptual Design Report, Volume 2: The Physics Program for DUNE at LBNF*, [1512.06148](#).

- [2] HYPER-KAMIOKANDE collaboration, *Hyper-Kamiokande Design Report*, [1805.04163](#).
- [3] T. Bhattacharya, V. Cirigliano, S.D. Cohen, A. Filipuzzi, M. Gonzalez-Alonso, M.L. Graesser et al., *Probing Novel Scalar and Tensor Interactions from (Ultra)Cold Neutrons to the LHC*, *Phys. Rev. D* **85** (2012) 054512 [[1110.6448](#)].
- [4] C.C. Chang et al., *A per-cent-level determination of the nucleon axial coupling from quantum chromodynamics*, *Nature* **558** (2018) 91 [[1805.12130](#)].
- [5] T.P. Cheng and R.F. Dashen, *Is  $SU(2) \times SU(2)$  a better symmetry than  $SU(3)$ ?*, *Phys. Rev. Lett.* **26** (1971) 594.
- [6] M. Hoferichter, J. Ruiz de Elvira, B. Kubis and U.-G. Meißner, *High-Precision Determination of the Pion-Nucleon  $\sigma$  Term from Roy-Steiner Equations*, *Phys. Rev. Lett.* **115** (2015) 092301 [[1506.04142](#)].
- [7] Y. Aoki et al., *FLAG Review 2021*, [2111.09849](#).
- [8] R. Gupta, S. Park, M. Hoferichter, E. Mereghetti, B. Yoon and T. Bhattacharya, *The nucleon sigma term from lattice QCD*, [2105.12095](#).
- [9] USQCD collaboration, *Lattice QCD and Neutrino-Nucleus Scattering*, *Eur. Phys. J. A* **55** (2019) 196 [[1904.09931](#)].
- [10] R.J. Hill, P. Kammel, W.J. Marciano and A. Sirlin, *Nucleon Axial Radius and Muonic Hydrogen — A New Analysis and Review*, *Rept. Prog. Phys.* **81** (2018) 096301 [[1708.08462](#)].
- [11] F. Hug, K. Aulenbacher, S. Friederich, P. Heil, R. Heine, R. Kempf et al., *Status of the MESA ERL Project*, in *Proc. ERL'19*, no. 63 in ICFA Advanced Beam Dynamics Workshop on Energy Recovery Linacs, pp. 14–17, JACoW Publishing, Geneva, Switzerland, jun, 2020, [DOI](#).
- [12] D. Becker et al., *The P2 experiment*, *Eur. Phys. J. A* **54** (2018) 208 [[1802.04759](#)].
- [13] A1 collaboration, *High-precision determination of the electric and magnetic form factors of the proton*, *Phys. Rev. Lett.* **105** (2010) 242001 [[1007.5076](#)].
- [14] R. Pohl et al., *The size of the proton*, *Nature* **466** (2010) 213.
- [15] A. Antognini et al., *Proton Structure from the Measurement of  $2S - 2P$  Transition Frequencies of Muonic Hydrogen*, *Science* **339** (2013) 417.
- [16] W. Xiong et al., *A small proton charge radius from an electron–proton scattering experiment*, *Nature* **575** (2019) 147.
- [17] Y.-H. Lin, H.-W. Hammer and U.-G. Meißner, *Dispersion-theoretical analysis of the electromagnetic form factors of the nucleon: Past, present and future*, *Eur. Phys. J. A* **57** (2021) 255 [[2106.06357](#)].

- [18] K. Ottnad, *Excited states in nucleon structure calculations*, in *38th International Symposium on Lattice Field Theory*, 11, 2020 [2011.12471].
- [19] G.P. Lepage, *The Analysis of Algorithms for Lattice Field Theory*, in *Theoretical Advanced Study Institute in Elementary Particle Physics*, 6, 1989.
- [20] S. Gusken, *A Study of smearing techniques for hadron correlation functions*, *Nucl. Phys. B Proc. Suppl.* **17** (1990) 361.
- [21] APE collaboration, *Glueball Masses and String Tension in Lattice QCD*, *Phys. Lett. B* **192** (1987) 163.
- [22] G.M. von Hippel, B. Jäger, T.D. Rae and H. Wittig, *The Shape of Covariantly Smeared Sources in Lattice QCD*, *JHEP* **09** (2013) 014 [1306.1440].
- [23] G.S. Bali, S. Collins and A. Schafer, *Effective noise reduction techniques for disconnected loops in Lattice QCD*, *Comput. Phys. Commun.* **181** (2010) 1570 [0910.3970].
- [24] E. Shintani, R. Arthur, T. Blum, T. Izubuchi, C. Jung and C. Lehner, *Covariant approximation averaging*, *Phys. Rev. D* **91** (2015) 114511 [1402.0244].
- [25] A. Stathopoulos, J. Laeuchli and K. Orginos, *Hierarchical probing for estimating the trace of the matrix inverse on toroidal lattices*, 1302.4018.
- [26] A.S. Gambhir, A. Stathopoulos and K. Orginos, *Deflation as a Method of Variance Reduction for Estimating the Trace of a Matrix Inverse*, *SIAM J. Sci. Comput.* **39** (2017) A532 [1603.05988].
- [27] L. Giusti, T. Harris, A. Nada and S. Schaefer, *Frequency-splitting estimators of single-propagator traces*, *Eur. Phys. J. C* **79** (2019) 586 [1903.10447].
- [28] D. Djukanovic, T. Harris, G. von Hippel, P.M. Junnarkar, H.B. Meyer, D. Mohler et al., *Isvector electromagnetic form factors of the nucleon from lattice QCD and the proton radius puzzle*, *Phys. Rev. D* **103** (2021) 094522 [2102.07460].
- [29] T. Draper, R.M. Woloshyn and K.-F. Liu, *Electromagnetic Properties of Nucleons From Lattice QCD*, *Phys. Lett. B* **234** (1990) 121.
- [30] EUROPEAN TWISTED MASS COLLABORATION collaboration, *Nucleon form factors with dynamical twisted mass fermions*, *PoS LATTICE2008* (2008) 139 [0811.0724].
- [31] Y.-C. Jang, R. Gupta, H.-W. Lin, B. Yoon and T. Bhattacharya, *Nucleon electromagnetic form factors in the continuum limit from (2+1+1)-flavor lattice QCD*, *Phys. Rev. D* **101** (2020) 014507 [1906.07217].
- [32] Y.-C. Jang, R. Gupta, B. Yoon and T. Bhattacharya, *Axial Vector Form Factors from Lattice QCD that Satisfy the PCAC Relation*, *Phys. Rev. Lett.* **124** (2020) 072002 [1905.06470].

- [33] RQCD collaboration, *Nucleon axial structure from lattice QCD*, *JHEP* **05** (2020) 126 [1911.13150].
- [34] C. Alexandrou et al., *Nucleon axial and pseudoscalar form factors from lattice QCD at the physical point*, *Phys. Rev. D* **103** (2021) 034509 [2011.13342].
- [35] M.T. Hansen and H.B. Meyer, *On the effect of excited states in lattice calculations of the nucleon axial charge*, *Nucl. Phys. B* **923** (2017) 558 [1610.03843].
- [36] B.C. Tiburzi, *Chiral Corrections to Nucleon Two- and Three-Point Correlation Functions*, *Phys. Rev. D* **91** (2015) 094510 [1503.06329].
- [37] O. Bar, *Nucleon-pion-state contribution to nucleon two-point correlation functions*, *Phys. Rev. D* **92** (2015) 074504 [1503.03649].
- [38] O. Bar,  *$N\pi$ -state contamination in lattice calculations of the nucleon axial form factors*, *Phys. Rev. D* **99** (2019) 054506 [1812.09191].
- [39] O. Bar and H. Colic,  *$N\pi$ -state contamination in lattice calculations of the nucleon electromagnetic form factors*, *Phys. Rev. D* **103** (2021) 114514 [2104.00329].
- [40] L. Maiani, G. Martinelli, M.L. Paciello and B. Taglienti, *Scalar Densities and Baryon Mass Differences in Lattice QCD With Wilson Fermions*, *Nucl. Phys. B* **293** (1987) 420.
- [41] S.J. Dong, K.F. Liu and A.G. Williams, *Lattice calculation of the strangeness magnetic moment of the nucleon*, *Phys. Rev. D* **58** (1998) 074504 [hep-ph/9712483].
- [42] S. Capitani, M. Della Morte, G. von Hippel, B. Jäger, A. Jüttner, B. Knippschild et al., *The nucleon axial charge from lattice QCD with controlled errors*, *Phys. Rev. D* **86** (2012) 074502 [1205.0180].
- [43] J.R. Green, J.W. Negele, A.V. Pochinsky, S.N. Syritsyn, M. Engelhardt and S. Krieg, *Nucleon electromagnetic form factors from lattice QCD using a nearly physical pion mass*, *Phys. Rev. D* **90** (2014) 074507 [1404.4029].
- [44] S. Capitani, M. Della Morte, D. Djukanovic, G. von Hippel, J. Hua, B. Jäger et al., *Nucleon electromagnetic form factors in two-flavor QCD*, *Phys. Rev. D* **92** (2015) 054511 [1504.04628].
- [45] S. Capitani, M. Della Morte, D. Djukanovic, G.M. von Hippel, J. Hua, B. Jäger et al., *Isovector axial form factors of the nucleon in two-flavor lattice QCD*, *Int. J. Mod. Phys. A* **34** (2019) 1950009 [1705.06186].
- [46] J. He et al., *Detailed analysis of excited state systematics in a lattice QCD calculation of  $g_A$* , 2104.05226.
- [47] K. Ottnad, D. Djukanovic, T. Harris, H.B. Meyer, G. von Hippel and H. Wittig, *Improved analysis of nucleon isovector charges and twist-2 matrix elements on CLS  $N_f = 2 + 1$  ensembles*, in *38th International Symposium on Lattice Field Theory*, 10, 2021 [2110.10500].

- [48] NUCLEON MATRIX ELEMENTS (NME) collaboration, *Precision Nucleon Charges and Form Factors Using 2+1-flavor Lattice QCD*, [2103.05599](#).
- [49] R.J. Hill and G. Paz, *Model independent extraction of the proton charge radius from electron scattering*, *Phys. Rev. D* **82** (2010) 113005 [[1008.4619](#)].
- [50] T. Bauer, J.C. Bernauer and S. Scherer, *Electromagnetic form factors of the nucleon in effective field theory*, *Phys. Rev. C* **86** (2012) 065206 [[1209.3872](#)].
- [51] A1 collaboration, *Electric and magnetic form factors of the proton*, *Phys. Rev. C* **90** (2014) 015206 [[1307.6227](#)].
- [52] J.J. Kelly, *Simple parametrization of nucleon form factors*, *Phys. Rev. C* **70** (2004) 068202.
- [53] C. Alexandrou, S. Bacchio, M. Constantinou, J. Finkenrath, K. Hadjiyiannakou, K. Jansen et al., *Proton and neutron electromagnetic form factors from lattice QCD*, *Phys. Rev. D* **100** (2019) 014509 [[1812.10311](#)].
- [54] E. Shintani, K.-I. Ishikawa, Y. Kuramashi, S. Sasaki and T. Yamazaki, *Nucleon form factors and root-mean-square radii on a  $(10.8\text{ fm})^4$  lattice at the physical point*, *Phys. Rev. D* **99** (2019) 014510 [[1811.07292](#)].
- [55] C. Alexandrou, K. Hadjiyiannakou, G. Koutsou, K. Ottnad and M. Petschlies, *Model-independent determination of the nucleon charge radius from lattice QCD*, *Phys. Rev. D* **101** (2020) 114504 [[2002.06984](#)].
- [56] PACS collaboration, *Calculation of the derivative of nucleon form factors in  $N_f=2+1$  lattice QCD at  $M_\pi=138\text{ MeV}$  on a  $(5.5\text{ fm})^3$  volume*, *Phys. Rev. D* **104** (2021) 074514 [[2107.07085](#)].
- [57] N. Hasan, J. Green, S. Meinel, M. Engelhardt, S. Krieg, J. Negele et al., *Computing the nucleon charge and axial radii directly at  $Q^2 = 0$  in lattice QCD*, *Phys. Rev. D* **97** (2018) 034504 [[1711.11385](#)].
- [58] PARTICLE DATA GROUP collaboration, *Review of Particle Physics*, *PTEP* **2020** (2020) 083C01.
- [59] H. Akaike, *A new look at the statistical model identification*, *IEEE Transactions on Automatic Control* **19** (1974) 716.
- [60] W.I. Jay and E.T. Neil, *Bayesian model averaging for analysis of lattice field theory results*, 2020.
- [61] J. Green, S. Meinel, M. Engelhardt, S. Krieg, J. Laeuchli, J. Negele et al., *High-precision calculation of the strange nucleon electromagnetic form factors*, *Phys. Rev. D* **92** (2015) 031501 [[1505.01803](#)].

- [62] R.S. Sufian, Y.-B. Yang, A. Alexandru, T. Draper, J. Liang and K.-F. Liu, *Strange Quark Magnetic Moment of the Nucleon at the Physical Point*, *Phys. Rev. Lett.* **118** (2017) 042001 [1606.07075].
- [63] R.S. Sufian, Y.-B. Yang, J. Liang, T. Draper and K.-F. Liu, *Sea Quarks Contribution to the Nucleon Magnetic Moment and Charge Radius at the Physical Point*, *Phys. Rev. D* **96** (2017) 114504 [1705.05849].
- [64] D. Djukanovic, K. Ottnad, J. Wilhelm and H. Wittig, *Strange electromagnetic form factors of the nucleon with  $N_f = 2 + 1$   $O(a)$ -improved Wilson fermions*, *Phys. Rev. Lett.* **123** (2019) 212001 [1903.12566].
- [65] C. Alexandrou, S. Bacchio, M. Constantinou, J. Finkenrath, K. Hadjiyiannakou, K. Jansen et al., *Nucleon strange electromagnetic form factors*, *Phys. Rev. D* **101** (2020) 031501 [1909.10744].
- [66] C. Alexandrou, S. Bacchio, M. Constantinou, K. Hadjiyiannakou, K. Jansen and G. Koutsou, *Quark flavor decomposition of the nucleon axial form factors*, *Phys. Rev. D* **104** (2021) 074503 [2106.13468].